JOURNAL OF APPLIED ELECTROCHEMISTRY 8 (1978) 445–454

Solid-state storage batteries

C. C. LIANG*, A. V. JOSHI†, N. E. HAMILTON

P. R. Mallory and Co. Inc., Laboratory for Physical Science, Northwest Industrial Park, Burlington, Mass. 01803, USA

Received 5 December 1977

Investigations were conducted to study the feasibility of a solid-state battery system for storage applications. During the development of various high energy density solid-state batteries we noted that the solid electrolyte material, LiI dispersed in large surface area Al_2O_3, has a high ionic conductivity at elevated temperatures, (for example $0{\cdot}1\ \Omega^{-1}\ cm^{-1}$ at 300° C) and is suitable for high-rate storage battery applications. In solid-state battery systems both the electrodes and electrolytes are in the solid state under the operating conditions of the battery. The absence of any liquid phase makes the individual cell containers unnecessary in a multicell battery resulting in a simplified battery structure and increased package efficiency. Furthermore, no material compatibility problem is encountered in the system. As a result, the solid-state battery system has excellent charge retention characteristics and a long projected operating life. Solid-state test cells, Li–Si/LiI(Al_2O_3)/TaS_2/Ta, Li–Si/LiI(Al_2O_3/TiS_2/Ti and Li–Si/LiI(Al_2O_3)/TiS_2, Sb_2S_3, Bi were constructed and subjected to discharge–charge cycle tests at 300 ± 10° C, at $13{\cdot}7\ mA\ cm^{-2}$. Preliminary test results demonstrated that these solid-state battery systems are rechargeable and may be suitable for both load levelling and/or vehicle propulsion. From the considerations of material availability and cost and operational efficiencies it was concluded that the Li–Si/LiI(Al_2O_3)/TiS_2, Sb_2S_3, Bi system is most suitable among the three systems studied for the development of practical storage batteries. Preliminary design studies showed that practical energy densities of $200\ W\,h\,kg^{-1}$ and $520\ W\,h\ l^{-1}$ can be realized with the Li–Si/TiS_2, Sb_2S_3, Bi storage batteries.

1. Introduction

During the development of various high energy density solid-state batteries [1–3] we noted that the solid electrolyte, LiI dispersed in large surface area Al_2O_3, has a high ionic conductivity at elevated temperatures, $0{\cdot}1\ \Omega^{-1}\ cm^{-1}$ at 300° C, and is suitable for high-rate applications. In view of the strong interest in recent years in high energy density secondary batteries for load levelling and vehicle propulsion we extended our investigations to the study of rechargeable solid-state systems for use in storage batteries which operate at elevated temperatures.

In the solid-state battery system both the electrodes and the electrolyte are in the solid state under the operating conditions. The absence of any liquid phase (solution or fused-salt electrolytes and/or molten electrodes) makes the individual cell containers unnecessary in a multicell battery resulting in a simplified battery structure and increased package efficiency with respect to the active components. Furthermore, no material compatibility problem is encountered in a properly selected system. As a result, the solid-state battery system has excellent charge retention characteristics and a long operating life.

The present investigation was carried out to study the feasibility of several solid-state battery systems for storage battery applications. The preliminary results of these studies are discussed in this paper.

2. Solid electrolyte material

The solid electrolyte material was prepared using anhydrous LiI and high surface area Al_2O_3 (ALCOA H151) according to the procedures

* Present Address: Wilson Greatbatch Ltd, 10 000 Wehrle Drive, Clarence, New York 14031.
† Present Address: ESB Inc., Yardley, Pennsylvania.

reported previously [3]. A well-blended mixture of anhydrous LiI (50–60 mol%) and high surface area Al_2O_3 was heated at 500 ± 50° C for about 17 hours in a helium-filled Vacuum Atmospheres dry box. After the heat treatment the electrolyte was allowed to cool to room temperature and pulverized in an alumina ball mill for use.

The total conductivity of the LiI(Al_2O_3) solid electrolyte was determined using a Li/LiI(Al_2O_3)/Li conductivity cell. The cell was constructed according to the following procedure.

A weighed amount of LiI(Al_2O_3) powder was pressed to 100 000 lb in^{-2} (3500 kg cm^{-2}) in a 1·524 cm diameter steel die to form a pellet. After the thickness of the pellet had been measured while in the steel die, thin Li electrodes with steel current collectors were pressed on both surfaces of the pellet to form the conductivity cell. The cell was sealed in a stainless steel case with a glass-to-metal seal for resistance measurements. The electrical connections were made by welding the current collectors to the centre post of the glass-to-metal seal and the steel case, respectively. No spring pressure was used in the cell assembly. The resistance of the pellet was measured by means of a General Radio conductance bridge at 1000 Hz. It was also determined from the potential drop between the two lithium electrodes upon passing a direct current. The results of the d.c. measurements are in excellent agreement with those obtained from the a.c. measurements (within ± 2%). The conductivity of the LiI(Al_2O_3) solid electrolyte was calculated from the measured resistance and the physical dimensions of the pellet.

Fig. 1 shows the Arrhenius plot for the conductivity of the LiI(Al_2O_3) solid electrolyte in the temperature range between − 50° C and + 350° C. It is noted that the activation energy for the conduction process in the temperature range of − 50° C to + 300° C is 0·4 eV and that the conductivity is about 0·1 $(\Omega\,cm)^{-1}$ at 300° C. One of the desirable physical characteristics of the LiI(Al_2O_3) solid electrolyte is that the formation of a dense pellet does not require a high temperature sintering process. The electrolyte pellet can be formed by pressing powder at room temperature.

For the electronic conductivity measurements the Wagner polarization technique [4] was used.

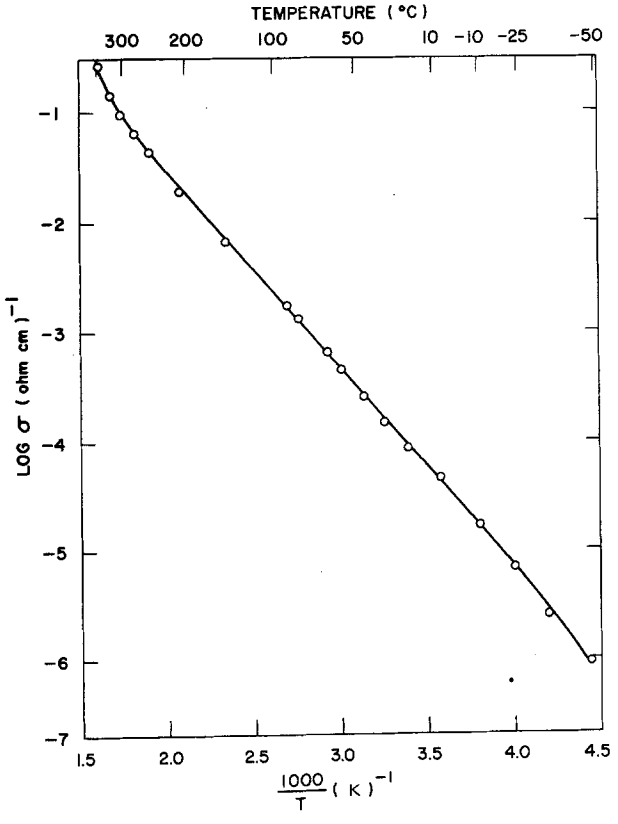

Fig. 1. Conductivity of the LiI(Al_2O_3) solid electrolyte as a function of temperature.

A polarization cell, Li/LiI(Al_2O_3)/Pt was constructed for these measurements. The Li/LiI(Al_2O_3)/Pt cell was polarized using a mercury battery with a voltage divider as a constant-potential source. The polarization potential was monitored by a Keithley 610B electrometer and the current in response to the polarization potential was monitored across a precision resistor using a Dana model 5500 digital voltmeter.

When a potential, E, which is lower than the decomposition potential of the electrolyte is applied to the polarization cell with the Pt electrode being positive, Li^+ ions move toward the Li electrode. Since E is lower than the decomposition potential and Pt does not supply Li^+ ions, a depletion of Li^+ ions results at the Pt–LiI(Al_2O_3) interface. Under steady-state conditions the current flow is then only due to electrons or electron holes. Wagner showed [4] that the total electronic current, I, which passes through the polarization cell under steady-state conditions is given by

$$I = I_e + I_h = \frac{RTA}{LF}\left\{\sigma_e^0\left[1-\exp\left(\frac{-EF}{RT}\right)\right] + \sigma_h^0\left[\exp\left(\frac{EF}{RT}\right)-1\right]\right\} \quad (1)$$

where I_e and I_h represent the currents due to electrons and holes, respectively; A and L are the cross-sectional area and the length of the electrolyte, respectively; R is the gas constant; F, the Faraday constant; and T, the absolute temperature. The electronic conductivities due to electrons and holes in LiI(Al_2O_3) in equilibrium with Li are denoted by σ_e^0 and σ_h^0 respectively. Generally, the conductivity due either to electrons or to holes is predominant. Therefore,

$$I \cong I_e = \frac{RTA}{LF}\sigma_e^0\left[1-\exp\left(-\frac{EF}{RT}\right)\right] \quad \text{when } \sigma_e^0 \gg \sigma_h^0 \quad (2)$$

and

$$I \cong I_h = \frac{RTA}{LF}\sigma_h^0\left[\exp\left(\frac{EF}{RT}\right)-1\right] \quad \text{when } \sigma_h^0 \gg \sigma_e^0. \quad (3)$$

Under the condition that the applied potential, E, is sufficiently high so that $EF \gg RT$, Equations 2 and 3 may be simplified, respectively, to

$$I \cong I_e \cong \frac{RTA}{LF}\sigma_e^0 \quad (4)$$

$$I \cong I_h \cong \frac{RTA}{LF}\sigma_h^0 \exp\left(\frac{EF}{RT}\right). \quad (5)$$

According to Equations 4 and 5 the polarization current, I, is independent of the applied potential in the case of electron conduction while $\log I$ is a linear function of E in the case of hole conduction. The hole conductivity, σ_h^0 can be obtained from the intercept of the $\log I$ versus E plot. Fig. 2 shows the $\log I$ versus E plots at various temperatures for the Li/LiI(Al_2O_3)/Pt cell. The straight line plots show that the electronic conductivity of Li(Al_2O_3) in equilibrium with Li is primarily due to the mobility of holes, the values of σ_h^0 at various temperatures are shown in Table 1. It should be noted, however, that the values of σ_h^0 shown in Table 1 are those at zero applied voltage. In other words, the leakage current calculated on the basis of the σ_h^0 values would be that of a cell whose open-circuit voltage is zero, such as Li/LiI(Al_2O_3)/Li. In actual electrochemical cells the open-circuit voltage is not zero. Therefore, the leakage current is higher than that calculated from σ_h^0 [5, 6]. One way to determine the leakage

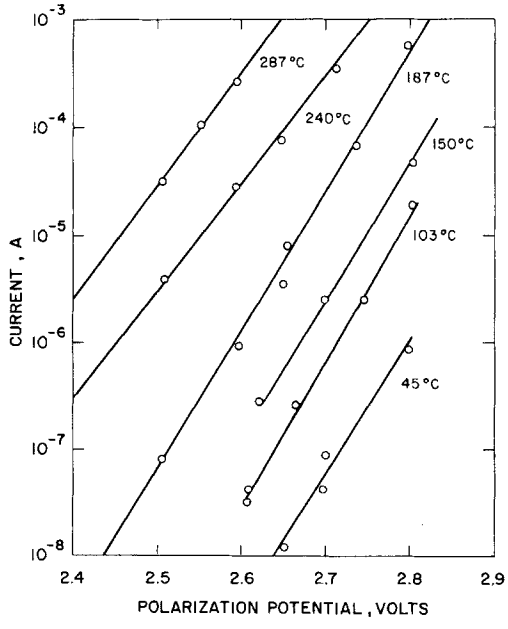

Fig. 2. d.c. polarization behaviour of the LiI(Al_2O_3) solid electrolyte in a Li/LiI(Al_2O_3)/Pt cell at various temperatures. Dimensions of the electrolyte pellet: 2 cm^2 × 0·05 cm.

Table 1. Electron hole conductivity of LiI(Al_2O_3) at various temperatures as determined from the intercept of the log I versus E plots (Fig. 3)

Temperature (° C)	*Electron hole conductivity* (σ_h^0) [$(\Omega\ cm)^{-1}$]
45	$< 10^{-40}$
103	$< 10^{-40}$
150	$< 10^{-40}$
187	5×10^{-39}
240	5×10^{-36}
287	5×10^{-29}
300	5×10^{-27}

current is to measure directly the current in the polarization cell at the open-circuit voltage of the electrochemical cell. The storage battery systems which we have investigated have open-circuit voltages in the range 2·4–2·5 V. Accordingly, we calculated the maximum leakage current for the LiI(Al_2O_3) solid electrolyte based on a 2·5 V open-circuit voltage and an electrolyte layer thickness of 0·5 mm (Fig. 3). It is noted from Fig. 3

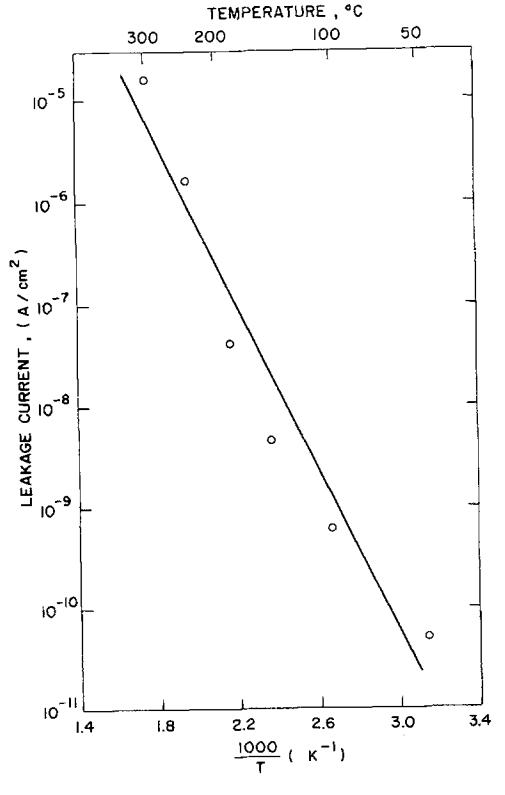

Fig. 3. Electronic leakage current of a 0·05 cm thick LiI(Al_2O_3) solid electrolyte layer at 2·5 V.

that the maximum leakage current due to electron flow through a 0·5 mm thick LiI(Al_2O_3) electrolyte is about 10^{-5} A cm^{-2} at 300° C and less than 10^{-11} A cm^{-2} at 25° C. These values are small compared with the ionic current capability of the cell. It was concluded that LiI(Al_2O_3) is an excellent solid electrolyte material in view of its high ionic conductivity, its low electronic conductivity, and its chemical compatibility with high energy density electrode materials.

3. Solid-state test batteries

Three types of test cells, Li–Si/LiI(Al_2O_3)/TaS_2/Ta, Li–Si/LiI(Al_2O_3)/TiS_2/Ti and Li–Si/LiI(Al_2O_3)/TiS_2, Sb_2S_3, Bi were constructed and subjected to the discharge–charge cycle tests. The selection of the Li–Si intermetallic compound as the anode material was based on its established rechargeability in fused-salt systems [7, 8]. Furthermore, unlike the pure Li metal which has a melting point of 186° C, the Li–Si intermetallic compound remains solid at the operating temperatures of 300–350° C. Therefore, no consideration had to be given to the containment of a liquid component and this resulted in a simple cell structure. The selection of the transition metal disulphides as the cathode material or cathode component was based on the reversibility characteristics between the metal sulphide and intercalated metal sulphide and the rechargeability of TiS_2 in non-aqueous liquid electrolyte systems [9–11].

The Li–Si intermetallic compound was prepared by heating a mixture of Li (78–82 mol%) and Si at 780 ± 20° C in a helium atmosphere for about one week. After the heat treatment the intermetallic compound which has the approximate composition $Li_{22}Si_5$ [12, 13] was cooled slowly to room temperature and pulverized for use. Commercial TaS_2 and TiS_2 (Ventron) were used as the cathode materials in the Li–Si/LiI(Al_2O_3)/TaS_2/Ta and Li–Si/LiI(Al_2O_3)/TiS_2/Ti cells, respectively. For the Li–Si/LiI(Al_2O_3)/TiS_2, Sb_2S_3, Bi cells the cathode was a mixture of well-blended 40 wt% TiS_2, 40 wt% Sb_2S_3 and 20 wt% Bi. Although the melting point of Bi (271° C) is lower than the operating temperature (300–350° C) of the test cells, no liquid metal was visible in the cathode mixture in either powder form or pressed-pellet form. Discharge

test results showed that no special container was necessary for the cathode mixture and the cathode mixture was indeed a solid under the test conditions.

The test cells were fabricated by pressing together the compounds sequentially at room temperature. In a 1·2 in (3·05 cm) diameter steel die, a weighed amount of cathode powder was dispersed on a Ti exmet (or a layer of Ta-powder in the case of TaS_2 cathode) levelled and pressed at about 5000 lb in^{-2} (350 kg cm^{-2}). A weighed amount of $LiI(Al_2O_3)$ electrolyte powder was then dispersed on the surface of the pre-pressed cathode, levelled and pressed at about 5000 lb in^{-2} (350 kg cm^{-2}). Finally, a weighed amount of Li–Si anode powder was dispersed and levelled on the pre-pressed electrolyte surface and a Ti current collector was placed on the anode. The total assembly was pressed at 50 000 lb in^{-2} (3500 kg cm^{-2}).

The capacity of the test cell was limited by the amount of cathode material. The anode was about 50% in excess. The geometric area of the electrode was 7·3 cm^2 and the thickness of the electrolyte layer was about 0·02 in (0·05 cm). The detailed structure of the test cell is shown in Fig. 4.

After fabrication, the test cells were hermetically sealed in stainless steel battery cases with glass-to-metal seals for discharge–charge cycle tests. The electrical contacts were made by welding the metal connecting tabs to the centre post of the glass-to-metal seal and the case, respectively. No spring pressure was used in the cell assembly. The purpose of the cycle tests was to determine the rechargeability of the system. No attempt was made to determine the optimal cell structure nor the number of cycles which can be realized with the present test cells.

3.1. *Li/LiI(Al_2O_3)//TaS_2/Ta test cells*

The test cells exhibited an open-circuit voltage of 2·5 V at 300 ± 10° C. The stoichiometric capacity was 250 mA h and the test cells were discharged and charged at a constant current of 0·1 A (13·7 mA cm^{-2}, *C*/2·5 rate) at 300 ± 10° C. Fig. 5 shows the discharge–charge curves of the Li–Si/TaS_2 cells. It is noted from Fig. 5 that the discharge curve after the tenth discharge–charge cycle is identical to that of the freshly constructed cell (first discharge) indicating the rechargeability of the Li–Si/TaS_2 system.

3.2. *Li–Si/LiI(Al_2O_3)//TiS_2/Ti test cells*

The Li–Si/TiS_2 test cells exhibited an open-circuit voltage of 2·4 V. The stoichiometric capacity of the cathode was 240 mA h. The test cells were discharged and charged at 0·1 A (13·7 mA cm^{-2}, *C*/2·4 rate) at 300 ± 10° C. The rechargeability of the system was demonstrated by the three discharge–charge cycles (Fig. 6). However, severe polarization losses were noted during discharge and charge processes.

3.3. *Li–Si/LiI(Al_2O_3)//TiS_2, Sb_2S_3, Bi test cells*

The Li–Si/TiS_2, Sb_2S_3, Bi test cells exhibited an open-circuit voltage of 2·4 V similar to that of the Li–Si/TiS_2 cells. Under similar discharge–charge conditions (0·1 A at 300 ± 10° C) the polarization loss of the Li–Si/TiS_2, Sb_2S_3, Bi test cells was

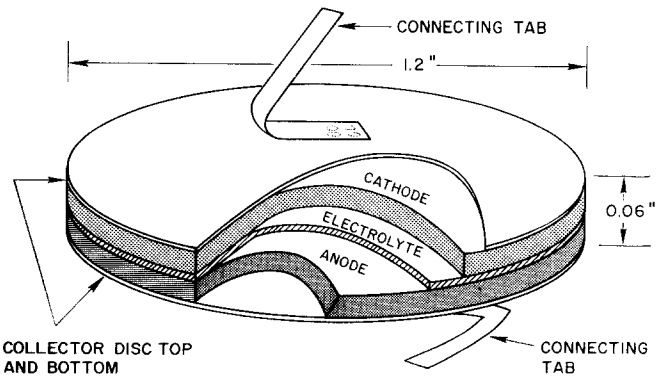

Fig. 4. Detailed interior structure of the Li–Si/LiI(Al_2O_3)/TiS_2, Sb_2S_3, Bi laboratory test cell.

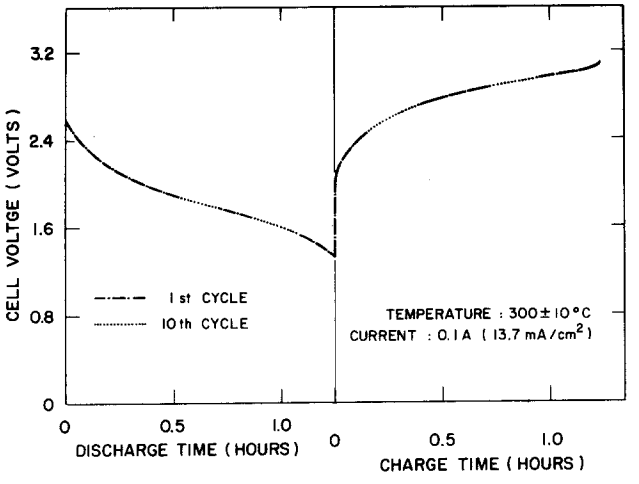

Fig. 5. Discharge–charge cycle tests of the Li–Si/LiI(Al_2O_3)/TaS_2/Ta test cell. Geometric area of the electrodes, 7·3 cm^2: stoichiometric capacity, 250 mA h: discharge–charge temperature, 300 ± 10° C: discharge–charge current, 0·1 A (C/2·5 rate): discharged capacity, 125 mA h.

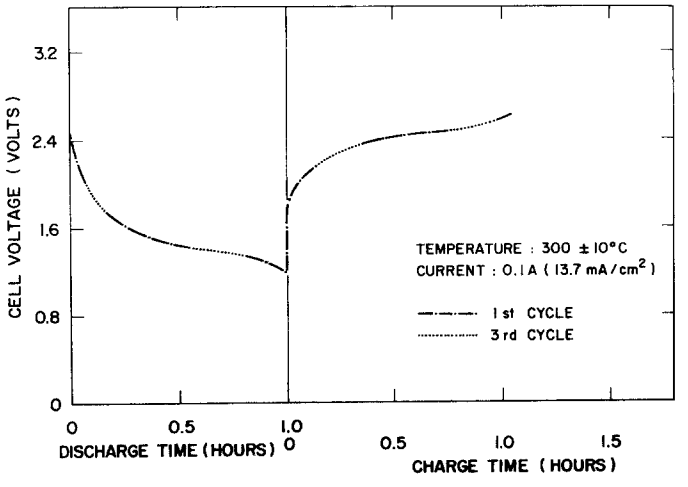

Fig. 6. Discharge–charge cycle tests of the Li–Si/LiI(Al_2O_3)/TiS_2/Ti test cell. Geometric area of the electrodes, 7·3 cm^2: stoichiometric capacity, 240 mA h: discharge–charge temperature, 300 ± 10° C: discharge–charge current, 0·1 A (C/2·4 rate): discharged capacity, 100 mA h.

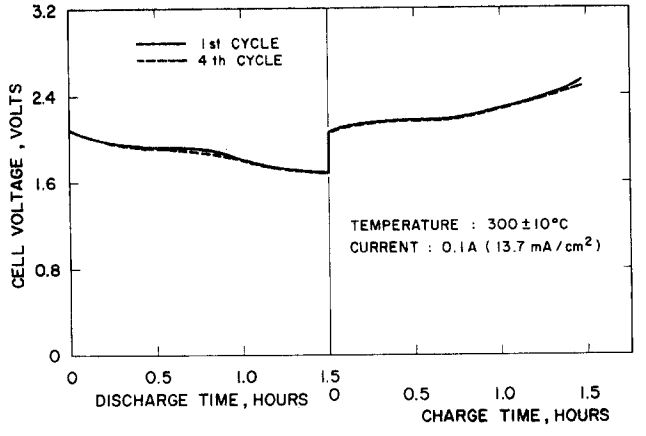

Fig. 7. Discharge–charge cycle tests of the Li–Si/LiI(Al_2O_3)/TiS_2, Sb_2S_3, Bi test cell. Geometric area of the electrodes, 7·3 cm^2: stoichiometric capacity, 430 mA h: discharge–charge temperature, 300 ± 10° C: discharge–charge current, 0·1 A (C/4·3 rate): discharged capacity, 150 mA h.

considerably less than that of the Li–Si/TiS_2 cells. Fig. 7 shows the discharge–charge curves of the Li–Si/TiS_2, Sb_2S_3, Bi test cells with a cathode capacity of 430 mA h at 0·1 A (13·7 mA cm^{-2}, $C/4{\cdot}3$ rate) at 300 ± 10° C.

It is noted that the Li–Si/LiI(Al_2O_3)/TiS_2, Sb_2S_3, Bi test cell operated at a higher efficiency than the Li–Si/LiI(Al_2O_3)/TiS_2 test cell. Under similar discharge conditions the causes for the difference in discharge efficiencies between the two types of test cells have not been investigated. Nonetheless, it should be noted that the operating temperature (300 ± 10° C) is above the melting point of Bi. Although no liquid Bi was visible in the cathode in either powder form or pressed-pellet form, it is conceivable that liquid Bi is present in the cathode. The presence of liquid Bi may result in a 'plastic' cathode which could accomodate the volume change accompanying the intercalation of lithium into TiS_2 and maintain the interface contact between the cathode and the electrolyte.

4. Preliminary battery design

An examination of the preliminary discharge–charge test results revealed that the three solid-state systems are rechargeable. Furthermore both the Li–Si/TaS_2 and the Li–Si/TiS_2, Sb_2S_3, Bi systems operate at higher efficiencies than the Li–Si/TiS_2 system. From the material availability and cost viewpoints the TaS_2 cathode is less desirable than the TiS_2, Sb_2S_3, Bi cathode. Accordingly, we concluded that the Li–Si/TiS_2, Sb_2S_3, Bi system is the most suitable system for the development of practical storage batteries.

Based on the information available thus far we made a preliminary design and a cost analysis of a prototype battery based on the Li–Si/LiI(Al_2O_3)/TiS_2, Sb_2S_3, Bi system in order to demonstrate the potentiality of the system in storage-battery applications and to provide guidelines for further studies.

A prototype battery with a nominal energy of 72 kW h was used as the design model. Table 2 shows the projected characteristics of the prototype battery and the parameters on which the battery design was based.

The single cell is 24 in (61 cm) long, 3 in (7·6 cm) wide and 0·077 in (0·2 cm) thick and has a capacity of about 46 A h (0·64 A h in^{-2} or about 0·1 A h cm^{-2}). Thirty single cells, connected in series, form a 72 V battery module which is shown in Fig. 8. Twenty-four battery modules, connected in parallel and arranged in two tiers, form the battery. The battery (Fig. 9) is encapsulated in a steel case with a ceramic-to-metal seal. The nominal voltage and capacity of such a proposed prototype battery would be 72 V and 1100 A h, respectively. Assuming that the average discharge voltage is 50 V and the realizeable capacity is 1000 A h, the realizeable energy densities would

*Table 2. Characteristics of nominal 72 kW h prototype battery**

Type	*Dimensions* [cm (in)]	*Volume* [l (in^3)]	*Weight* (kg)	*Capacity* [A h stoichiometric (A h realizeable)]	*Voltage*† *(average)*	*Practical energy density*	
						(W h kg^{-1})	(W h l^{-1})
Unit cell	61 × 7·6 × 0·2 (24 × 3 × 0·077)	0·091 (5·5)	0·126	46 (41·7)	2·41 (1·67)	280	810
Battery module	61 × 7·6 × 6·2 (24 × 3 × 2·45)	2·89 (176)	9·45	46 (41·7)	72·3 (50)	220	730
Prototype battery	76 × 62 × 20 (30 × 24·3 × 8)	96 (5832)	258	1100 (1000)	72·3 (50)	200	520
Battery with heating elements and insulation	84 × 70 × 28 (33 × 27·3 × 11)	162 (9910)	291	1100 (1000)	72·3 (50)	170	310

* Based on the following parameters:
Anode: $Li_{22}Si_5$, density ≅ 0·85 g cm^{-3}; capacity g^{-1} ≅ 1·4 A h g^{-1} (assuming 70% stoichiometry)
Cathode: 40 wt% TiS_2, 40 wt% Sb_2S_3, 20 wt% Bi; density = 4·2 g cm^{-3}; capacity g^{-1} = 0·285 A h g^{-1} (assuming Li + TiS_2 → $LiTiS_2$ and 6 Li + Sb_2S_3 → $3Li_2S$ + 2Sb)
Electrolyte: LiI(Al_2O_3); density = 3 g cm^{-3}
† Open circuit voltage

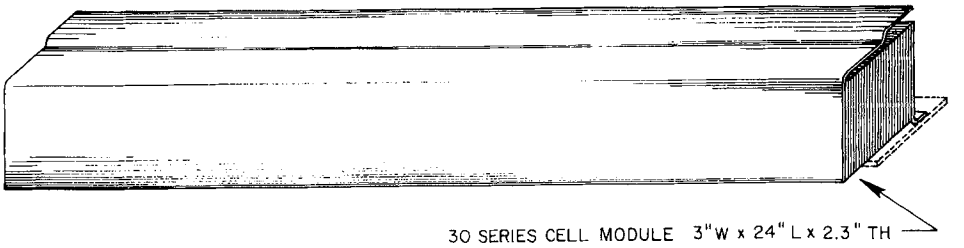

Fig. 8. Detailed structure of the 72 V, 46 A h battery module for the prototype battery.

be 200 W h kg^{-1} and 520 W h l^{-1} based on the weight (258 kg) and volume (96 l) of the battery.

No detailed discussion will be given of the temperature and heat management. However, heat exchangers, heating elements and insulation (1·5 in thick) were provided for the conceptual battery (Fig. 10). The inclusion of the heating elements and insulation layer would decrease the energy densities from 200 W h kg^{-1} and 520 W h l^{-1} to 170 W h kg^{-1} and 310 W h l^{-1}.

Table 3 shows an approximate material cost estimate. It is noted that the material cost was

*Table 3. Material cost analyses for the nominal 72 kW h prototype battery**

Unit	*Unit cost* ($ lb^{-1})	*Weight/battery* (lb)	*Cost/battery* ($)	*% total*	*Cost/kW h*† ($)
Electrolyte					
Li	11·60	1·77	20·53	2·11	0·41
I_2	2·59	32·38	83·86	8·63	1·66
Al_2O_3	0·16	22·08	3·53	0·36	0·07
			107·92		2·14
Anode					
Li	11·60	25·78	299·05	30·79	5·93
Si	0·51	66·30	33·81	3·48	0·67
Steel collector	0·16	44·20	7·07	0·73	0·14
			339·93		6·74
Cathode					
TiO_2	0·27	69·25	18·70	1·93	0·37
H_2S	0·10	60·41	6·04	0·62	0·12
Bi	7·50	49·36	370·20	38·11	7·35
Sb	1·58	70·72	111·73	11·50	2·22
S	0·03	29·47	0·88	0·09	0·02
Steel	0·14	66·30	9·28	0·96	0·21
			516·83		10·29
Case					
Shell	0·16	39·6	6·34	0·65	0·13
Insulation	0·02	18·1	0·36	0·04	0·01
			6·70		0·14
	Total material cost/battery = 971·38				
	† Material cost/kW h = 19·27				

* Material cost based on [14, 15]

† An estimated realizeable energy of 50·4 kW h was used in computing the material cost/kW h.

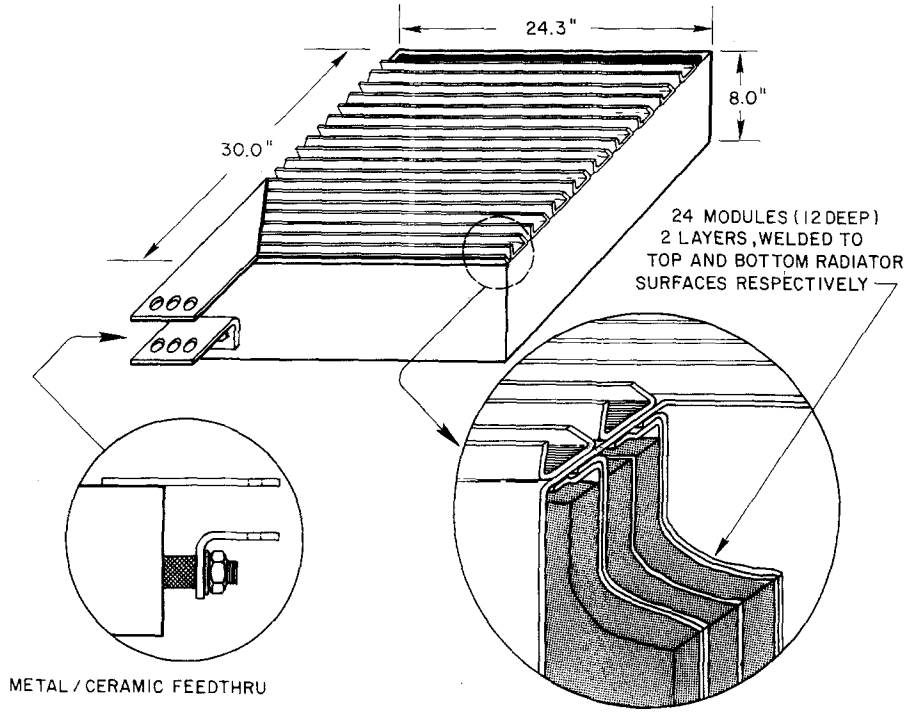

Fig. 9. Nominal 72 kW h prototype battery.

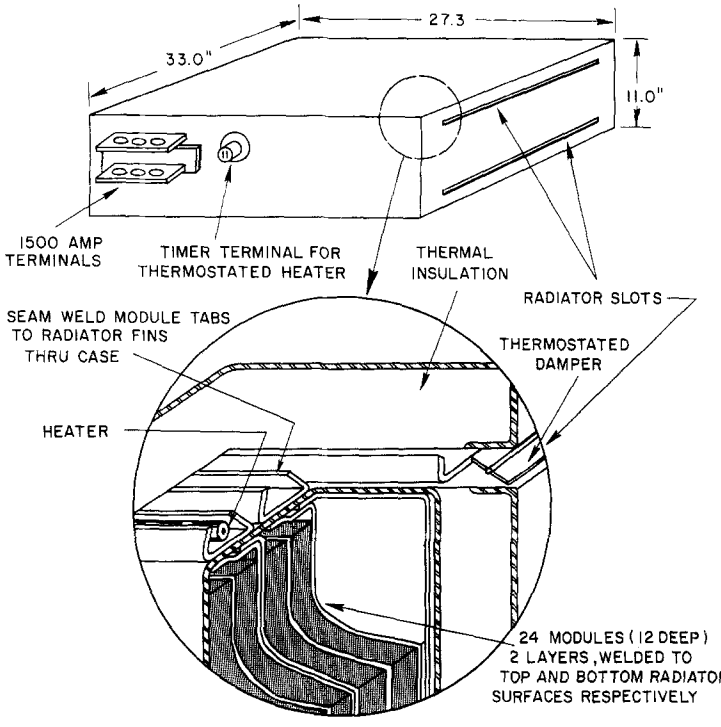

Fig. 10. Nominal 72 kW h prototype battery with insulation jacket.

based on the realizeable energy of the prototype battery (50 kW h) rather than the nominal energy (72 kW h). Based on the material cost of \$19·27/kW h it is estimated that the total cost (materials and labour) would be less than \$35/kW h.

References

[1] C. C. Liang, A. V. Joshi and L. H. Barnette, 27th Ann. Proc. Power Sources Conf. (1976) 141.

[2] C. C. Liang and L. H. Barnette, *J. Electrochem. Soc.* **123** (1976) 453.

[3] C. C. Liang, *ibid.* **120** (1973) 1289.

[4] C. Wagner, Proc. Int. Comm. Electrochem. Thermo. Kinetics 7 (1957) 361.

[5] A. V. Joshi and C. C. Liang, *J. Phys. and Chem. Solids* **36** (1975) 927.

[6] J. H. Kennedy, *J. Electrochem. Soc.* **124** (1977) 865.

[7] L. R. McCoy and L. A. Heredy, Proc. Intersoc. Energy Conversion Eng. Conf. **11** (1976) 485.

[8] J. S. Dunning, T. G. Bradley and E. J. Zeitner, Proc. Intersoc. Energy Conversion Eng. Conf. **11** (1976) 491.

[9] M. S. Whittingham, *J. Electrochem. Soc.* **123** (1976) 315.

[10] M. S. Whittingham and F. R. Gamble, *Mat. Res. Bull.* **10** (1975) 363.

[11] L. H. Gains, R. W. Francis, G. H. Newman and B. M. L. Rao, Proc. Intersoc. Energy Conversion Eng. Conf. **11** (1976) 418.

[12] R. A. Sharma and R. N. Seefurth, *J. Electrochem. Soc.* **123** (1976) 1763.

[13] R. N. Seefurth and R. A. Sharma, *ibid* **124** (1977) 1207.

[14] *American Metal Marketing News* (March, 1977).

[15] *Chemical Marketing Reporter* (June, 1977).